The Astrophysical Journal Letters, 770:L15 (6pp), 2013 June 10 doi:10.1088/2041-8205/770/1/L15

A HIGHLY ELONGATED PROMINENT LENS AT $z = 0.87$: FIRST STRONG-LENSING ANALYSIS OF EL GORDO

Adi Zitrin[1,6], Felipe Menanteau[2], John P. Hughes[2], Dan Coe[3], L. Felipe Barrientos[4], Leopoldo Infante[4], and Rachel Mandelbaum[5]

[1] Zentrum für Astronomie, Institut für Theoretische Astrophysik, Universität Heidelberg, Philosophenweg 12, D-69120 Heidelberg, Germany; adizitrin@gmail.com
[2] Department of Physics & Astronomy, Rutgers University, 136 Frelinghuysen Road, Piscataway, NJ 08854, USA
[3] Space Telescope Science Institute, 3700 San Martin Drive, Baltimore, MD 21218, USA
[4] Departamento de Astronomía y Astrofísica, Facultad de Física, Pontificia Universidad Católica, Casilla 306, Santiago 22, Chile
[5] Department of Physics, Carnegie Mellon University, Pittsburgh, PA 15213, USA
Received 2013 April 1; accepted 2013 May 15; published 2013 May 30

ABSTRACT

We present the first strong-lensing (SL) analysis of the galaxy cluster ACT-CL J0102−4915 (El Gordo), in recent *HST*/ACS images, revealing a prominent strong lens at a redshift of $z = 0.87$. This finding adds to the already-established unique properties of El Gordo: it is the most massive, hot, X-ray luminous, and bright Sunyaev–Zeldovich effect cluster at $z \gtrsim 0.6$, and the only "bullet"-like merging cluster known at these redshifts. The lens consists of two merging massive clumps, where, for a source redshift of $z_s \sim 2$, each clump exhibits only a small, separate critical area, with a total area of $0.69 \pm 0.11\square'$ over the two clumps. For a higher source redshift, $z_s \sim 4$, the critical curves of the two clumps merge together into one bigger and very elongated lens (axis ratio $\simeq$5.5), enclosing an effective area of $1.44 \pm 0.22\square'$. The critical curves continue expanding with increasing redshift so that for high-redshift sources ($z_s \gtrsim 9$) they enclose an area of $\sim 1.91 \pm 0.30\square'$ (effective $\theta_e \simeq 46''.8 \pm 3''.7$) and a mass of $6.09 \pm 1.04 \times 10^{14}\ M_\odot$. According to our model, the area of high magnification ($\mu > 10$) for such high-redshift sources is $\simeq 1.2\square'$, and the area with $\mu > 5$ is $\simeq 2.3\square'$, making El Gordo a compelling target for studying the high-redshift universe. We obtain a strong lower limit on the total mass of El Gordo, $\gtrsim 1.7 \times 10^{15}\ M_\odot$ from the SL regime alone, suggesting a total mass of roughly $M_{200} \sim 2.3 \times 10^{15}\ M_\odot$. Our results should be revisited when additional spectroscopic and *HST* imaging data are available.

Key words: dark matter – galaxies: clusters: general – galaxies: clusters: individual (ACT-CL J0102-4915)

Online-only material: color figures

1. INTRODUCTION

Massive galaxy clusters at high redshifts are rare beasts that hold important clues to the evolution of structure in the universe and can help probe the current ΛCDM paradigm (e.g., Harrison & Hotchkiss 2012; Waizmann et al. 2012; Zitrin et al. 2009a).

In this study we focus on ACT-CL J0102−4915, El Gordo, a high-redshift ($z = 0.87$), massive cluster discovered by the Atacama Cosmology Telescope (ACT) as the most significant Sunyaev–Zeldovich (SZ; Sunyaev & Zeldovich 1972) decrement in their survey area of $\sim$1000 deg^2 (Marriage et al. 2011; Menanteau et al. 2012; Hasselfield et al. 2013). The cluster was also detected by the South Pole Telescope (SPT) in their 2500 deg^2 survey as the highest significance SZ detection (Williamson et al. 2011). Additionally, recent results by the Planck Collaboration et al. (2013; see Figure 29 and related catalog therein) confirm that El Gordo is an extreme case, with the highest SZ-estimated mass at $z \gtrsim 0.65$. Menanteau et al. (2012) pursued an efficient multiwavelength follow-up using the Very Large Telescope (VLT), *Chandra*, and *Spitzer*. The spectra of 89 member galaxies yielded a cluster redshift, $z = 0.870$, and a velocity dispersion, $\sigma_{\rm gal} = 1321 \pm 106$ km s^{-1}. Their *Chandra* observations revealed a hot ($kT_X = 14.5 \pm 1.0$ keV) and X-ray luminous ($L_X = 2.19 \pm 0.11 \times 10^{45}$ erg s^{-1}) system with a complex morphology (see Menanteau et al. 2012); these values place El Gordo at the extreme massive end of all known clusters.

Menanteau et al. (2012) determined the mass of El Gordo to be $M_{200} = 2.16 \pm 0.32 \times 10^{15}\ M_\odot$, using multiple proxies such as the SZ effect, X-ray, and dynamics, making it the most massive and X-ray luminous galaxy cluster known at $z > 0.6$. Additionally, *Chandra* and VLT/FORS2 optical data revealed that El Gordo is undergoing a major merger between two components with a mass ratio of approximately 2:1; the most plausible direction for the merger inferred from the structures seen in the X-ray emission (see Menanteau et al. 2012) is along the NW–SE axis. To our knowledge, El Gordo is the only "bullet"-like cluster known to date at $z > 0.6$.

Due to the improvement of lens modeling techniques, *Hubble Space Telescope* (*HST*) imaging, and the studies of the high-redshift universe through cluster lenses (e.g., Kneib et al. 2004; Bradley et al. 2008, 2012; Richard et al. 2011; Bradač et al. 2012; Zheng et al. 2012; Zitrin et al. 2012b; Coe et al. 2013), the lensing efficiency and magnification power of galaxy clusters have been increasingly studied in recent years, in pursuit of the best cosmic telescopes (e.g., Oguri & Blandford 2009; Fedeli et al. 2010; Meneghetti et al. 2010; Redlich et al. 2012; Wong et al. 2012; Zitrin et al. 2012a, 2013). The efficiency and magnifying capabilities of a lens depend on a variety of factors, such as the mass, ellipticity, concentration, mass profile, amount of substructure and its distance from the center, and degree of relaxation or merger, as well as the redshift of the lens (and source). Recent efforts have now established that there exists a particular class of prominent strong lenses, consisting of massive, mostly merging clusters (found at increasing redshifts) for which the critical curves of the several mass clumps and

[6] The mass model and parameters are publicly available at: ftp://wise-ftp.tau.ac.il/pub/adiz/ElGordo.

different substructures can merge together into a bigger lens, resulting also in a shallower inner mass profile with higher magnification power. In addition, it has also been shown that high elongation of the critical curves boosts the lensing efficiency since the source-plane caustics get relatively bigger, generating more multiple-image systems. We refer the reader to the following examples and related comprehensive studies (e.g., Fedeli et al. 2010; Meneghetti et al. 2010; Lapi et al. 2012; Giocoli et al. 2012; Sereno & Zitrin 2012; Paraficz et al. 2012; Redlich et al. 2012; Wong et al. 2012; Zitrin et al. 2009a, 2012a, 2013).

For example, following these conclusions, such merging or substructured clusters have been now prioritized and chosen for the pioneering Frontier Fields[7] program, set to detect the highest redshift galaxies magnified by cosmic telescopes, with the *HST*.

Here, we present the first strong-lensing (SL) analysis of El Gordo in recent *HST* imaging with the Advanced Camera for Surveys (ACS). This cluster fulfills the criteria of the strongest lenses known experiencing a major merger between two massive clumps and has a very elongated mass distribution, yet has an additional intriguing property: its high redshift ($z_l = 0.87$). For this lens redshift, the relative lensing distance, i.e., lens-to-source angular diameter distance over the source angular diameter distance, or D_{ls}/D_s, increases substantially for higher redshift sources (relative to lower redshift sources) resulting in relatively rapidly expanding critical curves, forming a useful lens for observing the high-z universe, as we shall show below. Throughout we adopt a concordance ΛCDM cosmology with ($\Omega_{\rm m0} = 0.3$, $\Omega_{\Lambda 0} = 0.7$, $H_0 = 100\,h$ km s^{-1} Mpc^{-1}, with $h = 0.7$), where $1'' = 7.71$ kpc at the redshift of El Gordo.

2. OBSERVATIONS AND DATA REDUCTION

El Gordo was imaged with the ACS on board the *HST* in the F625W, F775W, and F850LP bands, on 2012 September 19 (prop ID: 12755; PI: Hughes), with integration times of 2344 s, 2512 s, and 2516 s, respectively. The ACS data set consists of two contiguous pointings centered on the NW and SE clumps of the cluster with a rotation angle of approximately 55°. The data were first processed by the STScI ACS Calibration pipeline (CALACS), which included bias and dark subtraction, flat-fielding, counts-to-electrons conversion, and charge transfer efficiency (CTE) correction using the pixel-based method described in Ubeda et al. (2012).

The images were then processed using an updated version of APSIS (Blakeslee et al. 2003) to reject cosmic rays (CRs) and combine the images in each band into geometrically corrected, single-field drizzled images. Object detection, extraction, and integrated photometry were performed using SExtractor (Bertin & Arnouts 1996) catalogs, produced by the APSIS pipeline. Photometric redshift estimates were computed with the Bayesian Photometric Redshift package (Benítez 2000) using isophotal-corrected magnitudes, and the prior calibrated with the northern Hubble Deep Field (HDF; HDF-N) spectroscopic sample.

We also make partial use here of the discovery observations of El Gordo, which took place in 2009 December with the 4.1 m SOAR Telescope using the *griz* filter set, with exposure times of 540 s, 720 s, 2200 s, and 2200 s, respectively, and a typical seeing of $<0\farcs7$ (see Menanteau et al. 2012 for complete details). Subsequently, El Gordo was observed using the FORS2 on VLT providing redshifts for 123 objects (89 cluster members). In addition to the *HST* images which are our primary data set for the lensing analysis, we use these other data to both help choose cluster members and visually inspect multiple-image candidates, particularly in the SOAR g-band data, which cover bluer wavelengths than the ACS F625W filter.

3. STRONG-LENSING ANALYSIS OF EL GORDO

For the SL analysis of El Gordo, we first use the method outlined in Zitrin et al. (2009b) which adopts a light-traces-mass (LTM) assumption for both the galaxies and dark matter (DM), where the latter is simply a smoothed version of the former, and the two components are added together and supplemented by an external shear to allow for more freedom and higher elongation (see Broadhurst et al. 2005; Zitrin et al. 2009b for full details). This method has been successfully applied to a large number of clusters (e.g., Zitrin et al. 2011, 2012c, 2013; Merten et al. 2011; Coe et al. 2013; Zheng et al. 2012). Thanks to the LTM assumption and the low number of parameters, the initial model is already constrained well enough to aid in physically finding multiple images across the cluster field, which are then used to iteratively refine the model. With this method, along with a complementary examination by eye, we uncovered in El Gordo four secure sets of multiple images and five additional multiply imaged candidate systems.

After physically matching up multiple images with the LTM model, we then model the cluster with a more flexible parameterization, consisting of two elliptical Navarro–Frenk–White (eNFW) halos representing the two cluster-scale DM clumps, and adopting pseudo-isothermal elliptical mass distributions (PIEMDs) for the galaxies. This parameterization consists of a total of 10 fundamental parameters: $r^*_{\rm cut}$ and σ^*_0, the cutoff radius and velocity dispersion of a typical L^* galaxy, for the PIEMD galaxy models (e.g., Jullo et al. 2007); the scale radius r_s and the concentration parameter $c_{\rm vir}$, as well as the ellipticity and its position angle, for each of the two eNFW halos whose centers are fixed on the central galaxies of the SE and NW clumps, respectively. The best-fit solution is obtained via a long (several dozens of thousands steps) Monte Carlo Markov Chain (MCMC) minimization. We previously used this method in our recent work, where more complete details can be found (Zitrin et al. 2013 and references therein).

In total, we found 27 multiple images and candidates of 9 background sources (Table 1, Figures 1 and 2), all of which were previously unknown, except for the giant arc (images 2.1+2.2) noted by Menanteau et al. (2012) as a possible multiply lensed galaxy. All images *not* marked as candidates were used as constraints for the model: 25 images and internal distinctive knots of 4 sources. The multiple images uncovered are well detected in the bluest *HST*, F625W band and in the bluer, ground-based g band (Section 2), and thus cannot be at redshifts larger than $z_s \sim 4$. Due to the high redshift of the cluster, it is also not likely that they are at lower redshifts than $z_s \sim 1.5$, since the lensing efficiency for lower source redshifts is very low. System 3 is only marginally detected in the g band and thus is probably at a higher redshift than most of the other systems, around $z_s \sim 4$, as also supported by our initial LTM model. Using this fact as a prior on the photo-z of this system, we obtain a combined redshift and 95% confidence level (C.L.) of 4.16 [4.04–4.23] for system 3. These constraints allow us to construct an SL mass model with Bayesian estimates for the model variables, including the redshifts of the different multiply lensed sources. We thus fix the redshift of system 3

[7] http://www.stsci.edu/hst/campaigns/frontier-fields/

Table 1
Multiple Images and Candidates Found by Our LTM Method

Arc ID	R.A. (J2000.0)	Decl. (J2000.0)	phot-z [$z_{\rm min}$-$z_{\rm max}$]	$z_{\rm model}$	Δ pos ″	Comments
1.1a	01:02:53.293	-49:15:16.13	1.800 [1.613–2.810]	2.69 [1.15–3.38]	1.1	
1.2a	01:02:52.837	−49:15:18.02	1.700 [1.520–2.980]	···	4.8	
1.3a	01:02:55.422	−49:14:59.69	2.380 [1.880–2.690]	···	5.1	
1.1b	01:02:53.340	−49:15:16.00	1.180 [1.035–2.400]	···	1.0	
1.2b	01:02:52.772	−49:15:18.34	1.690 [1.511–2.320]	···	4.7	
1.3b	01:02:55.402	−49:15:00.01	2.400 [1.880–2.710]	···	5.1	
1.1c	01:02:53.489	−49:15:15.65	2.200 [1.987–3.310]	···	0.8	
1.2c	01:02:52.618	−49:15:19.32	2.800 [2.470–3.053]	···	4.1	
1.3c	01:02:55.331	−49:15:00.86	2.800 [2.540–3.053]	···	5.2	
2.1a	01:02:55.861	−49:15:51.94	2.210 [1.996–2.460]	2.11 [1.85–3.07]	1.5	
2.2a	01:02:56.760	−49:15:45.58	3.140 [2.864–3.416]	”	3.2	
2.3a	01:02:54.418	−49:16:04.20	2.510 [2.276–2.750]	”	2.4	
2.1b	01:02:55.704	−49:15:53.32	···	”	1.7	
2.2b	01:02:56.885	−49:15:45.06	···	”	1.3	
2.3b	01:02:54.467	−49:16:03.89	···	”	0.2	
2.1c	01:02:56.005	−49:15:50.81	···	”	1.3	
2.2c	01:02:56.584	−49:15:46.74	···	”	0.7	
2.3c	01:02:54.394	−49:16:04.18	···	”	0.6	
3.1	01:02:56.268	−49:15:06.60	4.160 [3.816–4.504]	4.16	1.4	sys fixed to $z_{\rm phot} = 4.16$
3.2	01:02:54.760	−49:15:19.18	1.100 [0.960–3.980]	”	0.9	$z_{\rm phot}$ 4.000 [3.420–4.333] using a prior (Section 3)
3.3	01:02:51.545	−49:15:38.02	0.900 [0.773–4.390]	”	2.2	$z_{\rm phot}$ 4.360 [4.003–4.717] using a prior (Section 3)
4.1	01:02:59.997	−49:15:49.11	1.690 [1.511–3.310]	2.15 [1.86–2.91]	6.1	
4.2	01:02:58.148	−49:16:21.50	2.240 [2.024–3.040]	”	3.0	
c4.3	01:02:58.178	−49:16:24.10	2.100 [1.893–3.060]	”	0.3	Probable radial counter image
4.4	01:02:55.362	−49:16:25.73	2.300 [2.080–3.120]	”	1.9	
4.5	01:02:56.610	−49:16:07.91	4.070 [3.732–4.408]	”	3.6	Blended with nearby galaxy
c5.1	01:02:59.612	−49:16:26.16	0.940 [0.811–1.130]	2.21 [1.91–4.04]	3.6	
c5.2	01:02:59.449	−49:16:27.81	0.920 [0.792–1.330]	”	1.7	
c5.3	01:02:54.942	−49:16:35.58	1.200 [1.053–1.450]	”	5.6	
c6.1	01:02:52.380	−49:15:00.91	3.100 [1.720–3.373]	2.12 [1.65–3.66]	4.7	
c6.2	01:02:54.167	−49:14:54.54	0.950 [0.820–1.420]	”	5.6	
c7.1	01:02:55.499	−49:16:06.89	0.900 [0.773–1.120]	2.01 [1.32–3.75]	2.6	
c7.2	01:02:54.938	−49:16:14.42	0.900 [0.773–1.190]	”	0.2	
c8.1	01:02:55.858	−49:16:07.13	1.750 [1.567–2.760]	1.86 [1.58–2.59]	2.8	
c8.2	01:02:55.222	−49:16:15.78	1.900 [1.707–3.270]	”	2.1	
c8.3	01:02:58.026	−49:15:51.33	1.440 [1.190–2.270]	”	0.8	
c9.1	01:02:56.309	−49:16:07.53	2.190 [1.977–3.150]	1.95 [1.28–2.75]	2.7	
c9.2?	01:02:55.179	−49:16:22.71	3.300 [2.320–3.587]	”	2.2	
c9.2?	01:02:55.652	−49:16:17.11	2.220 [1.910–2.910]	”	2.8	
c9.3	01:02:59.054	−49:15:52.92	2.300 [1.960–2.810]	”	4.5	

Notes. Column 1: arc ID. “c”-ID stands for the *candidate* for which the model-predicted location or identification *by eye* was ambiguous. For systems 1 and 2, we identify and use different parts of the images designated by their ID followed by a/b/c; Columns 2 and 3: R.A. and Decl. in J2000.0; Column 4: photometric redshift and 95% C.L.; Column 5: predicted and 95% C.L. redshift by the model; Column 6: reproduction distance of the image from its observed location, using a mean source position; Column 7: comments.

to $z_{\rm phot} = 4.16$, and allow the redshifts of the other systems (1, 2, and 4) to vary around their median photo-z value, with a flat prior. The resulting model redshift estimates are given in Table 1.

For the final model, the image-plane reproduction rms (χ^2) is 3″.2 (122.66), using only images (and their distinctive knots) referred to as secure. For the χ^2 we used a positional error of $\sigma_{\rm pos} = 1''.4$, which was found to be a reasonable value accounting for large-scale structure and matter along the line of sight (Jullo et al. 2010; D’Aloisio & Natarajan 2011; Host 2012). The multiple-image input comprises 25 constraints, where the number of degrees of freedom (DOF) is 23 yielding correspondingly $\chi^2/{\rm DOF} = 5.3$. These values are slightly higher than similar detailed lensing analyses, but are typical of complex or merging systems (e.g., Broadhurst et al. 2005; Limousin et al. 2012). Also, note that due to the relatively low number of constraints we did not leave the Brightest Cluster Galaxies (BCGs) or other bright members to be freely weighted nor allowed the NFW halo centers to vary, which often refine the fit. We note that with further careful analysis and additional *HST* observations particularly with a wider color range, more multiple-image systems are anticipated to be uncovered, and the mass model could be improved further.

3.1. Results and Discussion

In Figure 1, we show the resulting critical curves for different source redshifts. The critical area for systems 1, 2, and 4, estimated at a typical source redshift of $z_s \sim 2$–2.5, consists of two separate critical curves encircling the NW and SE mass peaks. The mass enclosed within this total critical area of

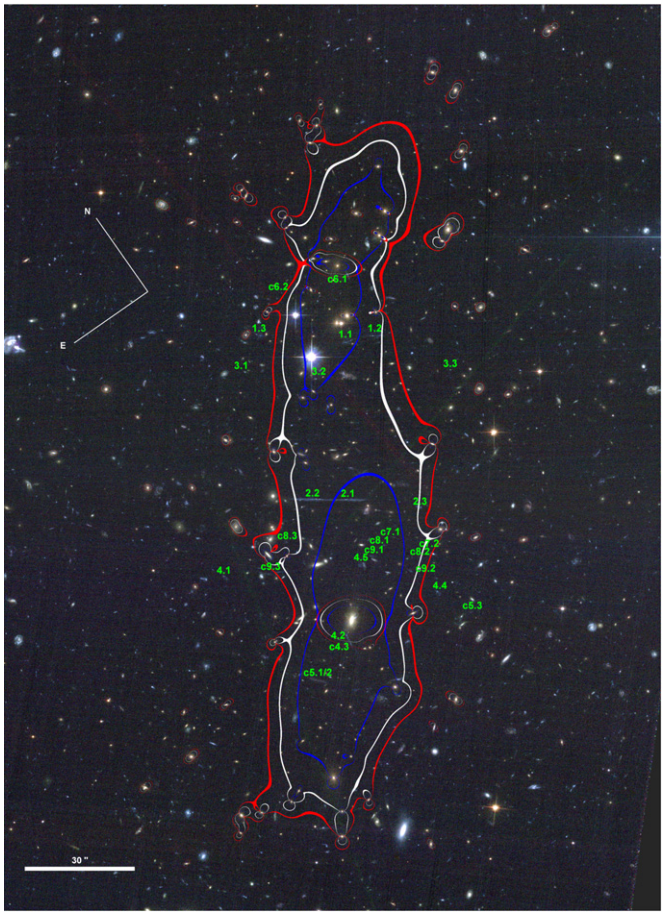

Figure 1. Critical curves for different source redshifts overlaid on a three-band *HST* image of El Gordo (RGB = [F850LP, F775W, F625W]; North is 35° counterclockwise of the positive *y*-axis). Using our unique LTM mass modeling technique (Zitrin et al. 2009b), we have been able to physically find the first 27 multiple images and candidates of at least 9 background sources, as labeled on the image ("c" stands for candidate). We then used these multiple-image constraints to model the cluster as two *e*NFW halos representing the DM, plus PIEMD parameterizations for the galaxies. The resulting critical curves overlaid in blue correspond roughly to systems 1, 2, and 4, at a typical redshift of $z_s \sim 2$–2.5. With increasing redshift the critical curves of the two clumps merge together into one bigger lens. Overlaid in white are the critical curves for a source at $z_s \sim 4$ (system 3), and the outer red critical curve corresponds to a high-redshift, $z_s \sim 9$, source.

(A color version of this figure is available in the online journal.)

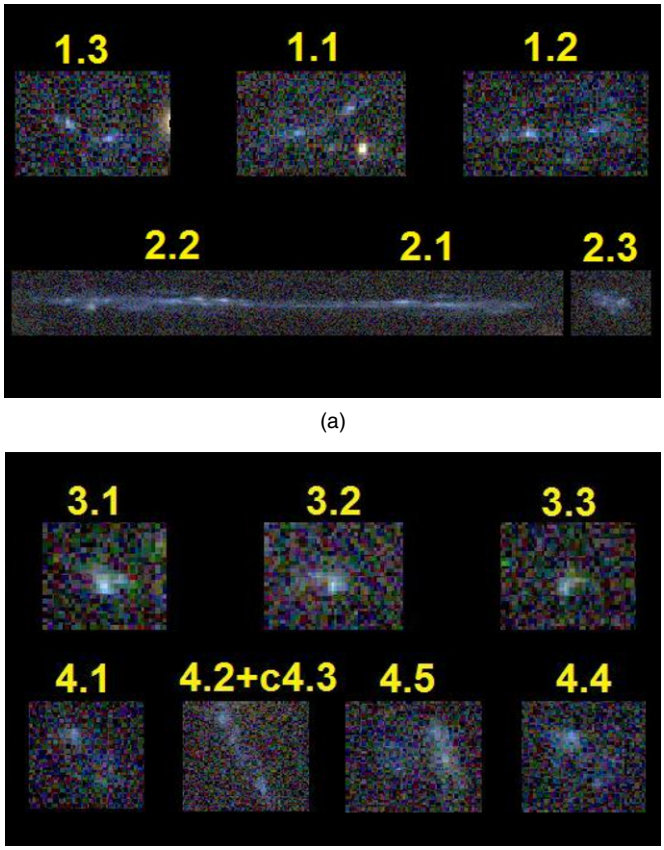

Figure 2. Zoomed-in examples of multiple images identified.

(A color version of this figure is available in the online journal.)

$0.69 \pm 0.11\square'$ is $3.12 \pm 0.53 \times 10^{14}\ M_\odot$ (errors correspond to 1σ). For system 3, at an estimated source redshift of $z_s \simeq 4.16$, the critical curves of the two clumps merge together into one bigger lens, enclosing an area of $1.44 \pm 0.22\square'$, and a mass of $5.06 \pm 0.86 \times 10^{14}\ M_\odot$. For a much higher source redshift, $z_s \sim 9$ for example, the critical curves enclose an area of $1.91 \pm 0.30\square'$ (effective Einstein radius of $\theta_e = \sqrt{(A/\pi)} \simeq 46''.8 \pm 3''.7$, or $\simeq 361 \pm 29$ kpc) and a mass of $6.09 \pm 1.04 \times 10^{14}\ M_\odot$. Additionally, we find that for this source redshift, the area of high magnification ($\mu > 10$) is $\simeq 1.15\square'$ and the area with $\mu > 5$ is $\simeq 2.25\square'$. These numbers mark El Gordo as a compelling cosmic lens for studying the high-redshift universe.

Our mass model suggests a mass ratio of ~1.5:1 between the SE and NW clumps, respectively (see Figure 3). Note that this is opposite to the mass ratio calculated in Menanteau et al. (2012), which found by velocity dispersion measurements that the NW clump was approximately twice as massive as the SE clump. However, clearly, the overall properties of a halo cannot be

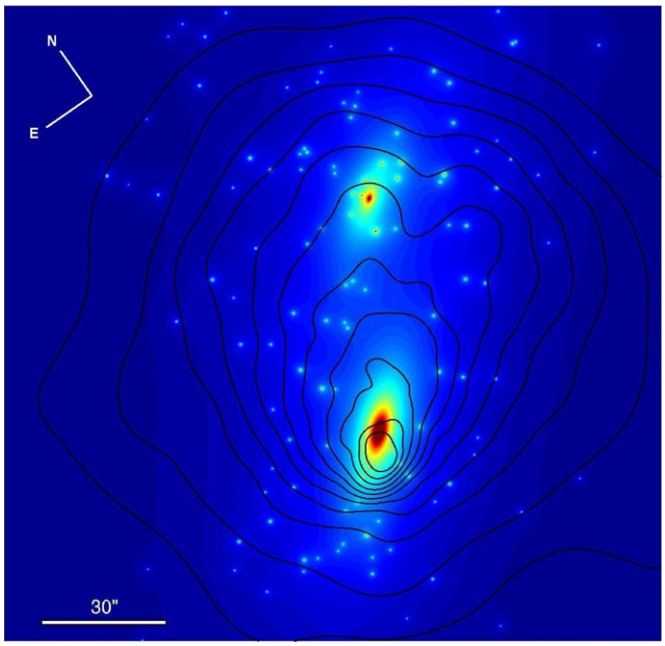

Figure 3. Surface density (κ) map of El Gordo (arbitrary color scale). Orientation is identical to that of Figure 1. Overlaid in black are the *Chandra* X-ray surface brightness contours from Menanteau et al. (2012; see also for discussion on the observed offsets from the X-ray peak).

(A color version of this figure is available in the online journal.)

deduced properly from the narrow SL regime alone, and so we leave further examination of the mass ratio to complementary weak-lensing studies.

To constrain the total mass of this cluster, we simply sum the mass within the field of view (FOV) presented in Figure 3, obtaining a mass of $\sim 1.7 \times 10^{15}\, M_\odot$ in that region which constitutes a strong lower limit for the total mass of this system. A simple NFW fit, for example, to the radial mass profile (of the mass map presented in Figure 3) centered on the optical midpoint between the two clumps suggests an overall mass of $M_{200} \simeq 2.3 \times 10^{15}\, M_\odot$. This simplified, rough estimate is in good agreement with the multi-method estimates of Menanteau et al. (2012); $M_{200} = 2.16 \pm 0.32 \times 10^{15}\, M_\odot$.

Recent statistical studies (e.g., Oguri & Blandford 2009; Fedeli et al. 2010; Meneghetti et al. 2010; Sereno & Zitrin 2012; Redlich et al. 2012; Wong et al. 2012; Zitrin et al. 2012a), and previous well-studied examples (e.g., MACS J0717.5+3745; Zitrin et al. 2009a; Limousin et al. 2012; the Bullet cluster Bradač et al. 2006; Paraficz et al. 2012; Abell 2744 Merten et al. 2011), have shown that massive merging clusters can form efficient lenses due to the substructured, spread out mass distribution which boosts the critical area, but also usually entails an overall shallower mass profile enhancing the magnification power (see also Coe et al. 2013; Zheng et al. 2012). In addition, Zitrin et al. (2013) recently showed that higher ellipticities enhance the lensing efficiency producing a larger number of multiple images per critical area, since the source-plane caustics are relatively bigger. Our analysis shows that El Gordo has a highly elongated mass distribution, or critical curves, with an axis ratio of approximately $\simeq$5.5, implying that more multiple images are likely to be uncovered in its field with deeper space imaging. Although Zitrin et al. (2013) have found a similarly high axis ratio for MACS J0416.1−2403, their numerical simulations also indicate that such high elongations are rare; only 4% of clusters with $M_{\rm vir} \geqslant 6 \times 10^{14}\, h^{-1}\, M_\odot$ exhibit such high elongations, highlighting the exceptional nature of El Gordo as a cosmic lens.

Using an up-to-date luminosity function (see Section 8 in Coe et al. 2013) convolved with our lens model, we predict that El Gordo should comprise a few dozen $z_s \sim 4$–6 galaxies, roughly three $z_s \sim 8$ galaxies, and possibly a few more at $z \gtrsim 9$ (with observations as deep as, e.g., 26.75 AB in *HST*'s F160W band, 10σ), taking into account two adjacent WFC3/IR pointings covering roughly the FOV seen in Figure 1. This is a fair number of high-z galaxies for a single cluster. For comparison, Bouwens et al. (2012) found three $z_s \sim 9$–10 galaxies over 19 Cluster Lensing And Supernova survey with Hubble (CLASH; Postman et al. 2012) clusters with a similar depth of $\sim$27 AB, and about $\sim 15\, z_s \sim 8$ galaxies are expected to be uncovered over the same fields (L. Bradley et al., in preparation).

4. SUMMARY

We presented the first SL study of El Gordo, in which we uncovered 27 multiple images and candidates of 9 background sources, revealing a prominent and highly elongated $z_l = 0.87$ lens efficient for lensing high-redshift sources. The resulting critical curves expand relatively rapidly with source redshift as may be expected from the redshift of the cluster, reaching a critical area of about $\sim 2\square'$ for $z_s \gtrsim 10$, and enclosing a mass of more than $6 \times 10^{14}\, M_\odot$. According to our model, for such high-z sources the area of high magnification ($\mu > 10$) is $\simeq 1.2\square'$, and the area with $\mu > 5$ is $\simeq 2.3\square'$. This rare lens shows again, as recently appreciated by various works, that the lensing properties of merging clusters are usually boosted (dependent on the mass, shape, and distance between the merging subclumps, e.g., Zitrin et al. 2013; see also Fedeli et al. 2010; Redlich et al. 2012; Wong et al. 2012).

We obtained a strong lower mass limit for El Gordo of $\sim 1.7 \times 10^{15}\, M_\odot$ from the SL regime alone, crudely suggesting a total mass of $M_{200} \simeq 2.3 \times 10^{15}\, M_\odot$ in agreement with Menanteau et al. (2012), $M_{200} = 2.16 \pm 0.32 \times 10^{15}\, M_\odot$. The existence of such massive clusters, in particular at redshifts as high as El Gordo's and above (e.g., Jee & Tyson 2009; Rosati et al. 2009; Gonzalez et al. 2012), can probe and provide interesting insight on structure formation in ΛCDM (e.g., Harrison & Hotchkiss 2012; Waizmann et al. 2012). Based on their aforementioned mass estimate, Menanteau et al. (2012) found that El Gordo, by itself, did not pose a strong challenge to ΛCDM. However, they noted that a more accurate mass estimate would be required to test this conclusion; if the mass were 3σ higher than their estimate, El Gordo would no longer be predicted to exist in ΛCDM, over the whole sky, with a 95% C.L. In this relation, we note that future spectroscopy and space imaging of this cluster should help to uncover more sets of multiple images, obtain more accurate redshifts, refine the mass model, and enhance the reliability of our results. We leave further discussion on the rarity of El Gordo to future papers including both strong and weak lensing, when the characteristics of this cluster over the entire observed spectrum and radius range are well understood.

In addition to testing cosmological models, cluster physics and structure evolution, based on its lensing properties outlined in this work, El Gordo is yet another compelling target to access the early universe searching for the first galaxies, in particular, in the era of recent $z \gtrsim 10$ galaxy discoveries (e.g., Bouwens et al. 2011, 2012; Coe et al. 2013; Zheng et al. 2012; Ellis et al. 2013) and the upcoming *HST* Frontier Fields science.

We greatly thank the reviewer of this work, Marceau Limousin, for valuable comments. A.Z. is supported by contract research "Internationale Spitzenforschung II/2-6" of the Baden Württemberg Stiftung. J.P.H. and F.M. are supported by *Chandra* grant No. GO2-13156X and *Hubble* grant No. HST-GO-12755.01-A. L.F.B. is supported by FONDECYT grant No. 1120676. ACS was developed under NASA contract NAS 5-32865. Results are based on observations made with the NASA/ESA *Hubble Space Telescope*, obtained from the data archive at the Space Telescope Science Institute. STScI is operated by the Association of Universities for Research in Astronomy, Inc. under NASA contract NAS 5-26555. This work is in part based on observations made with ESO Telescopes at the Paranal Observatory under program ID 086.A-0425.

REFERENCES

Benítez, N. 2000, ApJ, 536, 571
Bertin, E., & Arnouts, S. 1996, A&AS, 117, 393
Blakeslee, J. P., Anderson, K. R., Meurer, G. R., Benítez, N., & Magee, D. 2003, in ASP Conf. Ser. 295, Astronomical Data Analysis Software and Systems XII, ed. H. E. Payne, R. I. Jedrzejewski, & R. N. Hook (San Francisco, CA: ASP), 257
Bouwens, R., Bradley, L., Zitrin, A., et al. 2012, arXiv:1211.2230
Bouwens, R. J., Illingworth, G. D., Labbe, I., et al. 2011, Natur, 469, 504
Bradač, M., Clowe, D., Gonzalez, A. H., et al. 2006, ApJ, 652, 937
Bradač, M., Vanzella, E., Hall, N., et al. 2012, ApJL, 755, L7
Bradley, L. D., Bouwens, R. J., Ford, H. C., et al. 2008, ApJ, 678, 647
Bradley, L. D., Bouwens, R. J., Zitrin, A., et al. 2012, ApJ, 747, 3
Broadhurst, T., Benítez, N., Coe, D., et al. 2005, ApJ, 621, 53
Coe, D., Zitrin, A., Carrasco, M., et al. 2013, ApJ, 762, 32

D'Aloisio, A., & Natarajan, P. 2011, MNRAS, 411, 1628
Ellis, R. S., McLure, R. J., Dunlop, J. S., et al. 2013, ApJL, 763, L7
Fedeli, C., Meneghetti, M., Gottlöber, S., & Yepes, G. 2010, A&A, 519, A91
Giocoli, C., Meneghetti, M., Bartelmann, M., Moscardini, L., & Boldrin, M. 2012, MNRAS, 421, 3343
Gonzalez, A. H., Stanford, S. A., Brodwin, M., et al. 2012, ApJ, 753, 163
Harrison, I., & Hotchkiss, S. 2012, arXiv:1210.4369
Hasselfield, M., Hilton, M., Marriage, T. A., et al. 2013, arXiv:1301.0816
Host, O. 2012, MNRAS, 420, L18
Jee, M. J., & Tyson, J. A. 2009, ApJ, 691, 1337
Jullo, E., Kneib, J.-P., Limousin, M., et al. 2007, NJPh, 9, 447
Jullo, E., Natarajan, P., Kneib, J., et al. 2010, Sci, 329, 924
Kneib, J.-P., Ellis, R. S., Santos, M. R., & Richard, J. 2004, ApJ, 607, 697
Lapi, A., Negrello, M., González-Nuevo, J., et al. 2012, ApJ, 755, 46
Limousin, M., Ebeling, H., Richard, J., et al. 2012, A&A, 544, A71
Marriage, T. A., Acquaviva, V., Ade, P. A. R., et al. 2011, ApJ, 737, 61
Menanteau, F., Hughes, J. P., Sifón, C., et al. 2012, ApJ, 748, 7
Meneghetti, M., Fedeli, C., Pace, F., Gottlöber, S., & Yepes, G. 2010, A&A, 519, A90
Merten, J., Coe, D., Dupke, R., et al. 2011, MNRAS, 417, 333
Oguri, M., & Blandford, R. D. 2009, MNRAS, 392, 930
Paraficz, D., Kneib, J.-P., Richard, J., et al. 2012, arXiv:1209.0384
Planck Collaboration, Ade, P. A. R., Aghanim, N., et al. 2013, arXiv:1303.5089
Postman, M., Coe, D., Benítez, N., et al. 2012, ApJS, 199, 25
Redlich, M., Bartelmann, M., Waizmann, J.-C., & Fedeli, C. 2012, A&A, 547, A66
Richard, J., Kneib, J.-P., Ebeling, H., et al. 2011, MNRAS, 414, L31
Rosati, P., Tozzi, P., Gobat, R., et al. 2009, A&A, 508, 583
Sereno, M., & Zitrin, A. 2012, MNRAS, 419, 3280
Sunyaev, R. A., & Zeldovich, Y. B. 1972, CoASP, 4, 173
Ubeda, L., Anderson, J., & ACS Team., 2012, in American Astronomical Society Meeting Abstracts, 219, 241.03
Waizmann, J.-C., Redlich, M., & Bartelmann, M. 2012, A&A, 547, A67
Williamson, R., Benson, B. A., High, F. W., et al. 2011, ApJ, 738, 139
Wong, K. C., Ammons, S. M., Keeton, C. R., & Zabludoff, A. I. 2012, ApJ, 752, 104
Zheng, W., Postman, M., Zitrin, A., et al. 2012, Natur, 489, 406
Zitrin, A., Broadhurst, T., Barkana, R., Rephaeli, Y., & Benítez, N. 2011, MNRAS, 410, 1939
Zitrin, A., Broadhurst, T., Bartelmann, M., et al. 2012a, MNRAS, 423, 2308
Zitrin, A., Broadhurst, T., Rephaeli, Y., & Sadeh, S. 2009a, ApJL, 707, L102
Zitrin, A., Broadhurst, T., Umetsu, K., et al. 2009b, MNRAS, 396, 1985
Zitrin, A., Meneghetti, M., Umetsu, K., et al. 2013, ApJL, 762, L30
Zitrin, A., Moustakas, J., Bradley, L., et al. 2012b, ApJL, 747, L9
Zitrin, A., Rosati, P., Nonino, M., et al. 2012c, ApJ, 749, 97